Ion–Ion Interactions and Conduction Mechanism of Highly Conductive Fluorohydrogenate Ionic Liquids

AUTHOR(S):

Enomoto, Takeshi; Nakamori, Yoji; Matsumoto, Kazuhiko; Hagiwara, Rika

CITATION:

Enomoto, Takeshi ...[et al]. Ion–Ion Interactions and Conduction Mechanism of Highly Conductive Fluorohydrogenate Ionic Liquids. The Journal of Physical Chemistry C 2011, 115(10): 4324-4332

ISSUE DATE:

2011-03-17

URL:

http://hdl.handle.net/2433/259160

Ion-ion interactions and conduction mechanism of highly conductive fluorohydrogenate ionic liquids

Takeshi Enomoto, Yoji Nakamori, Kazuhiko Matsumoto, Rika Hagiwara*

Graduate School of Energy Science, Kyoto University, Yoshida, Sakyo-ku,

Kyoto 606-8501, Japan

* E-mail: k.matsumoto@ky7.ecs.kyoto-u.ac.jp

Abstract

Ion-ion interactions in highly conductive fluorohydrogenate ionic liquids (ILs) are discussed in this study. Low-temperature crystal structures of DMIm$(FH)_2F$ and DMIm$(FH)_3F$ (DMIm = 1,3-dimethylimidazolium) are determined by single-crystal X-ray diffraction to obtain location of each ion in the crystal lattice. Interaction energies between the imidazolium cation and fluorohydrogenate anions are evaluated with the aid of quantum mechanical calculations where the configuration of the ions are taken from the crystal structures of DMIm$(FH)_2F$ and DMIm$(FH)_3F$ as well as the previously determined EMImFHF (EMIm = 1-ethyl-3-methylimidazolium). The calculation suggests that the interaction energies are mainly dominated by electrostatic interactions as in the cases of other imidazolium salts and the low viscosity and high conductivity of fluorohydrogenate ILs are derived from their dynamic properties. The HF unit exchanging between fluorohydrogenate anions weakens the cation-anion interactions and produces smaller anionic diffusion species.

Keywords

Crystal structure, X-ray diffraction, Quantum mechanical calculation, Thermal analysis, hydrogen bonding, Electrolyte

Introduction

Ionic liquids (ILs) have attracted much attention and have been extensively investigated because of their unique properties. The properties often observed for ILs are extremely low vapor pressure, non-flammability, high thermal and electrochemical stabilities, and wide temperature range of liquid phase around room temperature.[1-8] Their potential applications include electrolytes in batteries, capacitors, and electrolytic bath and environmentally benign media for synthetic and catalytic reactions as well as extraction.[1-8] However, the high viscosity causing low conductivity of ILs is one of the problems preventing them from the practical application as electrolytes.[7,8]

Fluorohydrogenate ILs contain fluorohydrogenate anions ($(FH)_nF^-$) as anionic species and exhibit low viscosity and high conductivity.[9-16] For example, the viscosity and ionic conductivity at 25°C are 4.9 cP and 100 mS cm^{-1} for 1-ethyl-3-methylimidazolium ($EMIm^+$) fluorohydrogenate, $EMIm(FH)_{2.3}F$, and 5.1 cP and 110 mS cm^{-1} for 1,3-dimethylimidazolium ($DMIm^+$) fluorohydrogenate, $DMIm(FH)_{2.3}F$.[9,10] These values are considerably different from those for $EMImBF_4$ (34 cP and 13 mS cm^{-1} at 25°C)[17] with the similar anion size (*e.g.* molar volumes of 156 cm^3 mol^{-1} for both the cases) and make them attractive candidates as electrolytes.[7,18-20] The composition '*n*' of the vacuum-stable fluorohydrogenate ILs depends on the temperature of evacuation and is 2.3 at 25°C in most cases regardless of the cationic structures including imidazolium, pyridinium, pyrrolidinium, piperidinium, and phosphonium cations.[9-16] The anionic species in fluorohydrogenate ILs change depending on the HF composition '*n*' in $(FH)_nF^-$ (Figure 1), which is observed by IR spectroscopy, whereas no neutral HF is detectable in the liquid state. For example, the abundance ratio of $(FH)_2F^-$ to $(FH)_3F^-$ is 7:3 for $EMIm(FH)_{2.3}F$ from its composition.

Important factors to determine ionic conductivity of ILs are diffusion and dissociation of ions. The dissociation degree of ions is estimated by the ratio ($\Lambda_{imp}/\Lambda_{NMR}$), where Λ_{imp} is molar conductivity measured by electrochemical impedance method and Λ_{NMR} is molar conductivity calculated from a self-diffusion coefficient obtained by pulsed-gradient spin-echo NMR (PGSE-NMR) via the Nernst-Einstein relation.[21-25] Walden plot is a useful tool to evaluate the relationship between molar conductivity and viscosity. When the molar conductivity of an IL is plotted over the ideal line in the Walden plot, the IL

is considered to exhibit a special conduction mechanism such as Grotthus hopping.[26-28] In spite of the low viscosities and high molar conductivities of fluorohydrogenate ILs, their plots are on the ideal line, suggesting that the high conductivity of fluorohydrogenate ILs should be simply derived from their low viscosity.

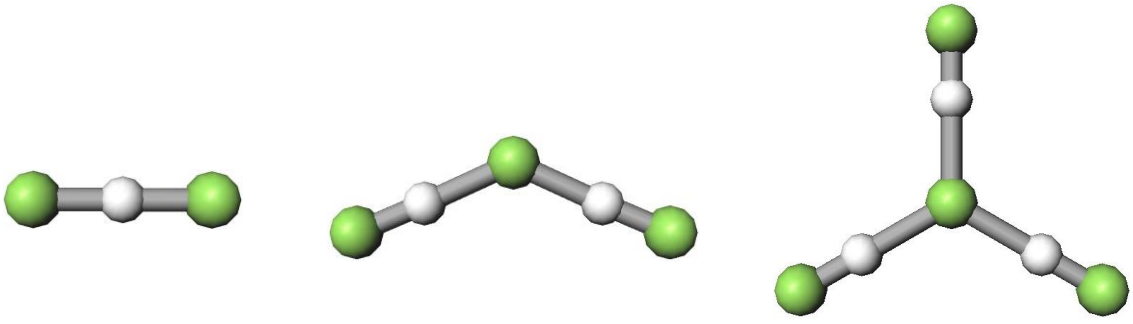

Figure 1. Fluorohydrogenate anions, $(FH)_nF^-$ (bifluoride ion (FHF^-), μ-fluoro-bis(fluorohydrogenate) ion ($(FH)_2F^-$), and μ_3-fluoro-tris(fluorohydrogenate) ion ($(FH)_3F^-$)).

Ion-ion interactions including hydrogen bonding in ILs are studied by quantum mechanical calculations.[29-32] It is considered that examining hydrogen-bonding environments is valuable to understand the characteristics of interaction and conformational influences of cations and anions on some properties such as lattice energy and melting point. From the close contact of the aromatic hydrogen atoms with electronegative atom in the anion in the crystal structures of 1-alkyl-3-methylimidazolium salts, the presence of the hydrogen bond is pointed out.[33-36] However, Tsuzuki *et al*. calculated interaction energies of the imidazolium cation with neighboring anions in the four crystal structures of 1-alkyl-3-methylimidazolium salts and the results suggested that the nature of the C−H···X interaction is considerably different from that of conventional hydrogen bonds; the interaction energy is determined mainly by the distance between the center of the imidazolium ring and anion and the orientation of the anion relative to the C−H bond does not greatly affect the size of the interaction energy.[32]

Although molecular dynamics simulations were performed on fluorohydrogenate ILs to obtain information of their high conductivity,[37-39] further understanding is required. In this study, ion

conduction mechanism in fluorohydrogenate ILs will be discussed from the ion-ion interaction in the solid and liquid states based on structural and physicochemical analyses. The former half of this study treats thermal and structural features of 1,3-dimethylimidazolium fluorohydrogenate salts ($DMIm(FH)_2F$ and $DMIm(FH)_3F$) in the solid state, followed by evaluation of static ion-ion interactions therein including hydrogen bonding using quantum mechanical calculations. In the latter half, ion-ion interactions in the liquid state are discussed and a conceivable ion diffusion model in fluorohydrogenate ILs is proposed.

Results and discussion

Thermal properties of $DMIm(FH)_nF$. Differential scanning calorimetric curves of $DMIm(FH)_{2.3}F$, $DMIm(FH)_2F$, and DMImFHF are shown in Figure 2. For $DMIm(FH)_{2.3}F$, two exothermic and two endothermic peaks are observed in the cooling and heating processes, respectively. Taking the composition and peak shape into account in the heating process, the peak at the lower temperature corresponds to melting of $DMIm(FH)_nF$ ($2 < n < 3$) at the eutectic composition, and the other peak (0°C at the top) is ascribed to melting of $DMIm(FH)_2F$ (*cf.* the phase diagrams of the MF-HF (M = alkali metal) salts[40,41]). The exothermic and endothermic peaks observed for $DMIm(FH)_2F$ are straightforwardly assigned to its freezing and melting. For DMImFHF, two exothermic and two endothermic peaks are observed. Based on the results of powder X-ray diffraction measurements (Figure 3), DMImFHF exhibits a solid-solid phase transition at 13°C, followed by the melting at 47°C.

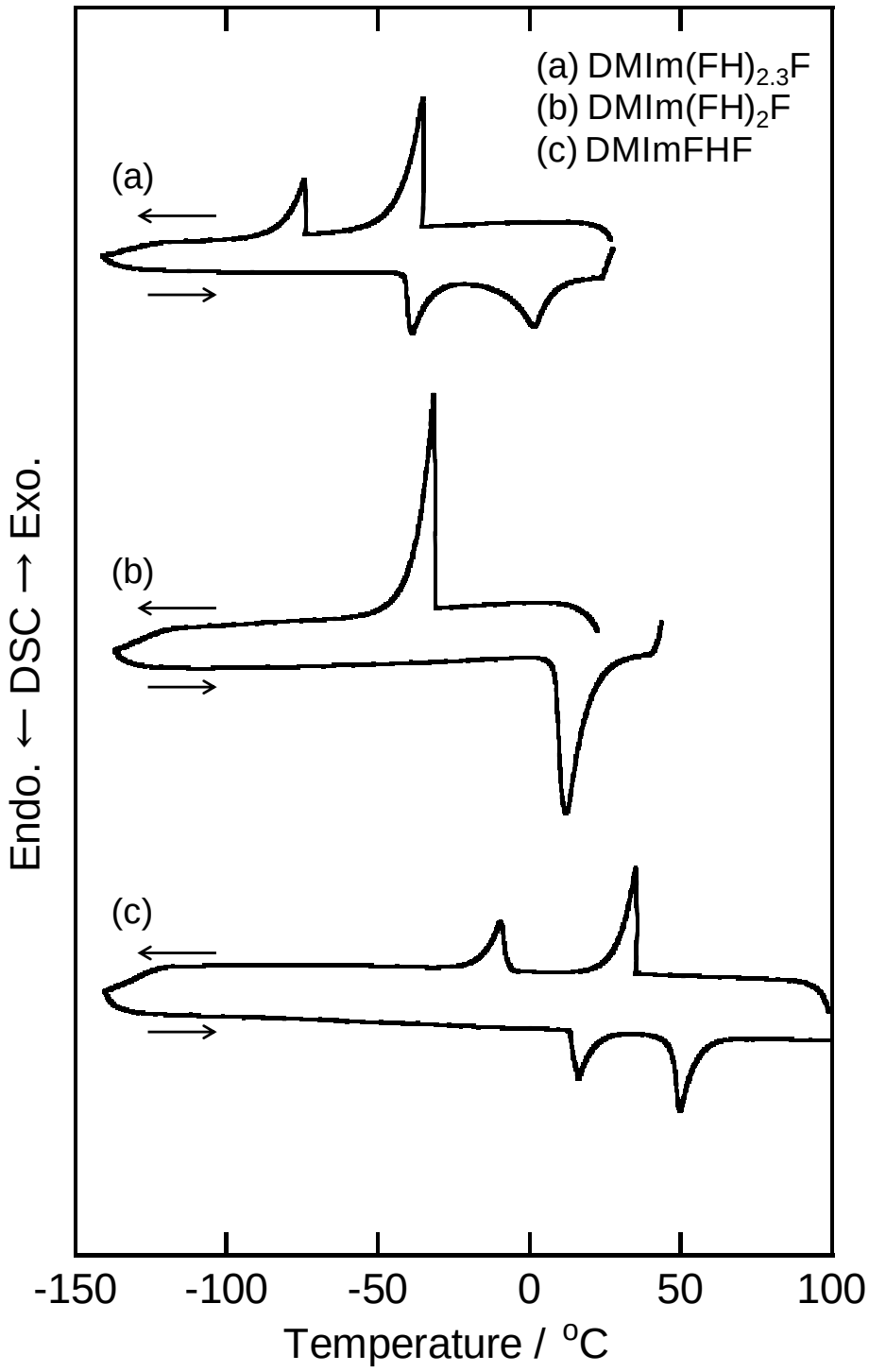

Figure 2. DSC curves of (a) $DMIm(FH)_{2.3}F$, (b) $DMIm(FH)_2F$, and (c) DMImFHF.

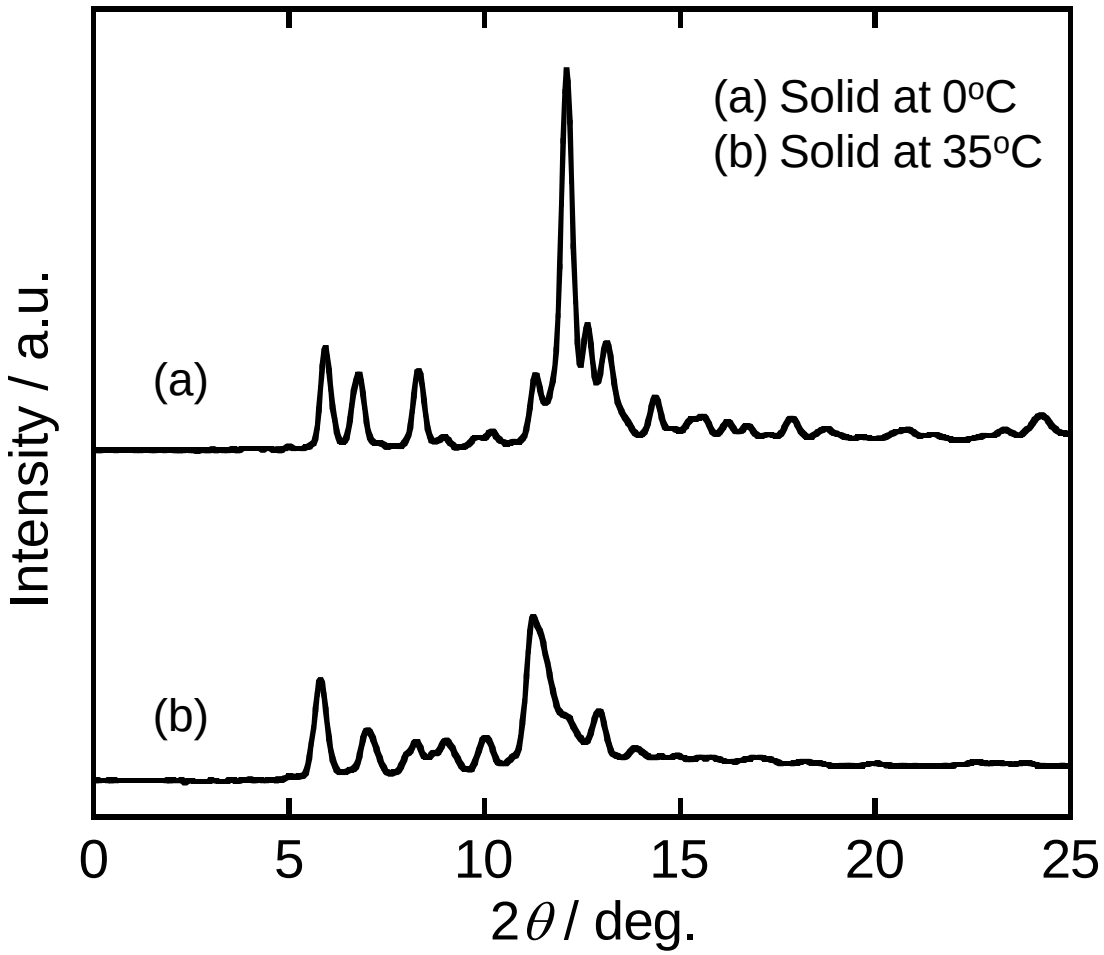

Figure 3. XRD patterns for two crystal phases of DMImFHF; (a) 0ºC and (b) 35ºC.

Crystal structures of DMIm(FH)$_2$F and DMIm(FH)$_3$F. Crystal structures of DMIm(FH)$_2$F and DMIm(FH)$_3$F were determined using single-crystal X-ray diffraction. These are the first crystal structures of dialkylimidazolium salts containing $(FH)_2F^-$ and $(FH)_3F^-$. The crystal structure of 1-ethyl-3-methylimidazolium bifluoride (EMImFHF) composed of $EMIm^+$ and FHF^- was already reported and the cations and anions form a unique layered structure.[33] Crystal data and refinement results for DMIm(FH)$_2$F and DMIm(FH)$_3$F are given in Table 1. Selected geometrical parameters for $DMIm^+$, $(FH)_2F^-$, and $(FH)_3F^-$ in the crystal structures are listed in Table 2 together with those of the optimized structures at MP2/aug-cc-pVTZ level (see Tables S1 and S2 in Supporting Information for the results at the other levels). The DMIm(FH)$_2$F and DMIm(FH)$_3$F salts crystallize in a triclinic lattice and a monoclinic lattice, respectively. Figures 4 and 5 give the asymmetric unit and packing diagram of DMIm(FH)$_2$F and DMIm(FH)$_3$F, respectively. The $DMIm^+$ cations adopt C_{2v} symmetry and their

geometrical parameters are in good agreement with those of $DMIm^+$ in the known crystal structures (*e.g.* $DMImPF_6$[42], $DMImN(SO_2CF_3)_2$[43], and $DMImOSO_2OCH_3$[44]) and also with those of the optimized geometry (Table 2).

Table 1. Single crystal structure data for $DMIm(FH)_2F$ and $DMIm(FH)_3F$

Salt	$DMIm(FH)_2F$	$DMIm(FH)_3F$
Formula	$C_5H_{11}N_2F_3$	$C_5H_{12}N_2F_4$
formula weight	156.151	176.1574
crystal system	Triclinic	Monoclinic
space group	*P*−1	$P2_1/n$
a / Å	7.357(4)	5.5980(2)
b / Å	8.151(5)	10.6076(4)
c / Å	8.444(5)	14.5523(7)
α / deg.	59.374(17)	90
β / deg.	61.691(14)	92.7130(10)
γ / deg.	65.709(16)	90
V / Å^3	373.9(5)	863.17(6)
Z	2	4
ρ_{calc} / g cm^{-3}	1.387	1.356
T / °C	−173	−173
μ / mm^{-1}	0.138	0.144
λ / Å	0.71073	0.71073
$R_1(F_o)^a$	0.0495	0.0338
$wR_2(F_o^2)^b$	0.0958	0.0888
Crystal size / mm^3	0.2×0.2×0.2	0.3×0.2×0.2
Extinction coefficient / 10^{-3}	23(9)	None

[a] $R_1 = \Sigma||F_o| - |F_c|| / \Sigma|F_o|$ for $I > 2\sigma(I)$.

[b] $wR_2 = \{\Sigma[w(F_o^2-F_c^2)^2] / \Sigma[w(F_o^2)^2]\}^{1/2}$ for $I > 2\sigma(I)$.

Table 2. Selected geometrical parameters for $DMIm(FH)_2F$ and $DMIm(FH)_3F$ with calculated geometrical parameters

Salt	$DMIm(FH)_2F$	$DMIm(FH)_3F$	MP2/aug-cc-pVTZ	
$DMIm^+$				
Bond lengths / Å				
N1−C2	1.346(6)	1.3263(14)	1.3391	
C2−N3	1.317(6)	1.3253(13)	1.3391	
N3−C4	1.378(6)	1.3798(13)	1.3704	
C4−C5	1.355(6)	1.3521(15)	1.3707	
C5−N1	1.359(6)	1.3782(14)	1.3704	
N1−C6	1.443(6)	1.4627(14)	1.4654	
N3−C7	1.482(6)	1.4646(13)	1.4654	
Bond angles / deg.				
N1−C2−N3	109.6(3)	108.71(9)	108.3	
C2−N3−C4	106.5(4)	108.80(9)	108.9	
N3−C4−C5	109.5(4)	106.76(9)	107.0	
C4−C5−N1	105.4(4)	107.08(9)	107.0	
C5−N1−C2	109.1(4)	108.65(9)	108.9	
C2−N1−C6	126.7(4)	125.26(9)	125.5	
C5−N1−C6	124.1(4)	126.08(9)	125.7	
C2−N3−C7	125.1(4)	125.09(9)	125.5	
C4−N3−C7	128.3(4)	126.10(9)	125.7	
$(FH)_nF^-$	$(FH)_2F^-$	$(FH)_3F^-$	$(FH)_2F^-$	$(FH)_3F^-$
Distance / Å				
F11−F12	2.333(4)	2.3822(10)	2.3499	2.4187
F11−F13	2.305(4)	2.3871(10)	2.3499	2.4187
F11−F14	−	2.4058(10)	−	2.4187
Bond angles / deg.				
F12−F11−F13	134.96(17)	108.75(4)	132.4	120.0
F13−F11−F14	−	115.72(4)	−	120.0
F14−F11−F12	−	133.18(4)	−	120.0

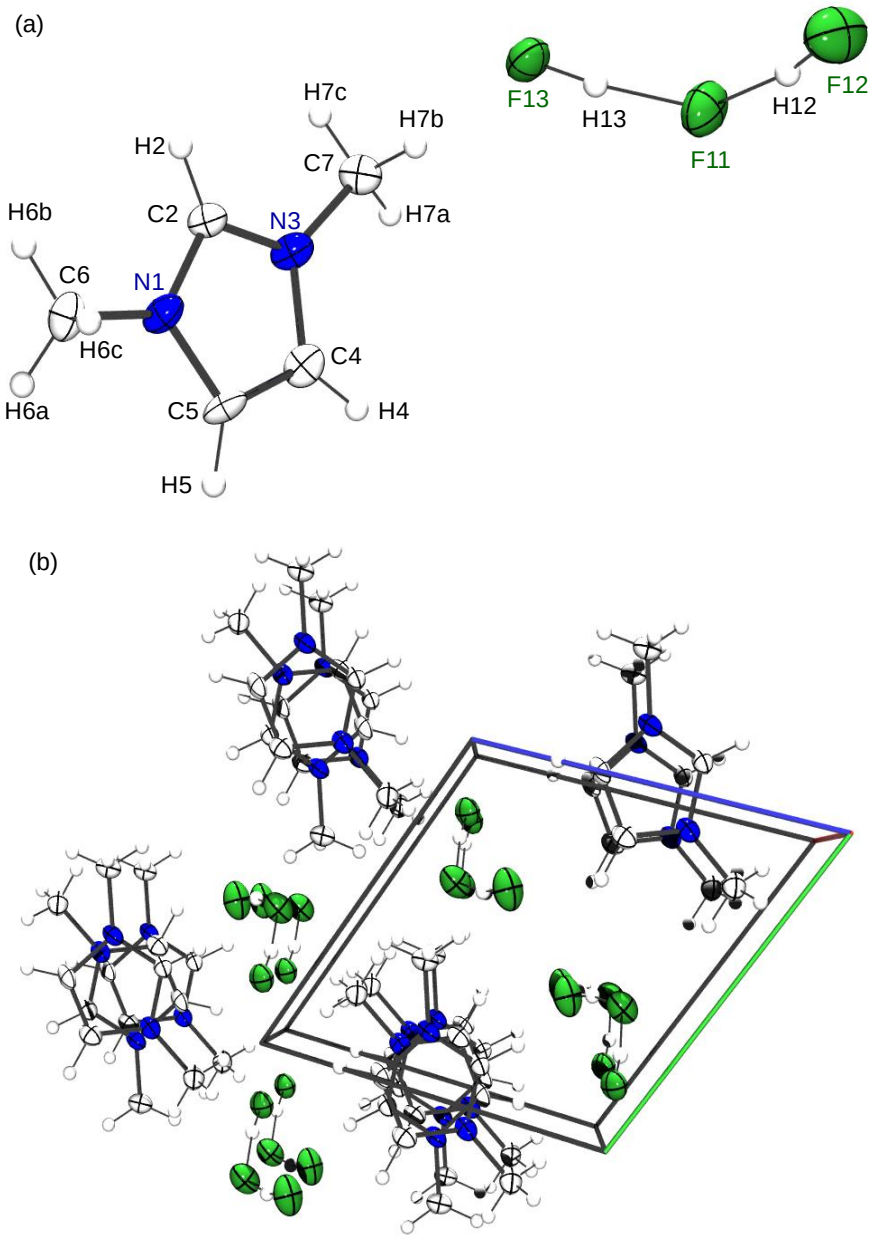

Figure 4. Crystal structure of DMIm(FH)$_2$F; (a) asymmetric unit and (b) Crystal packing.

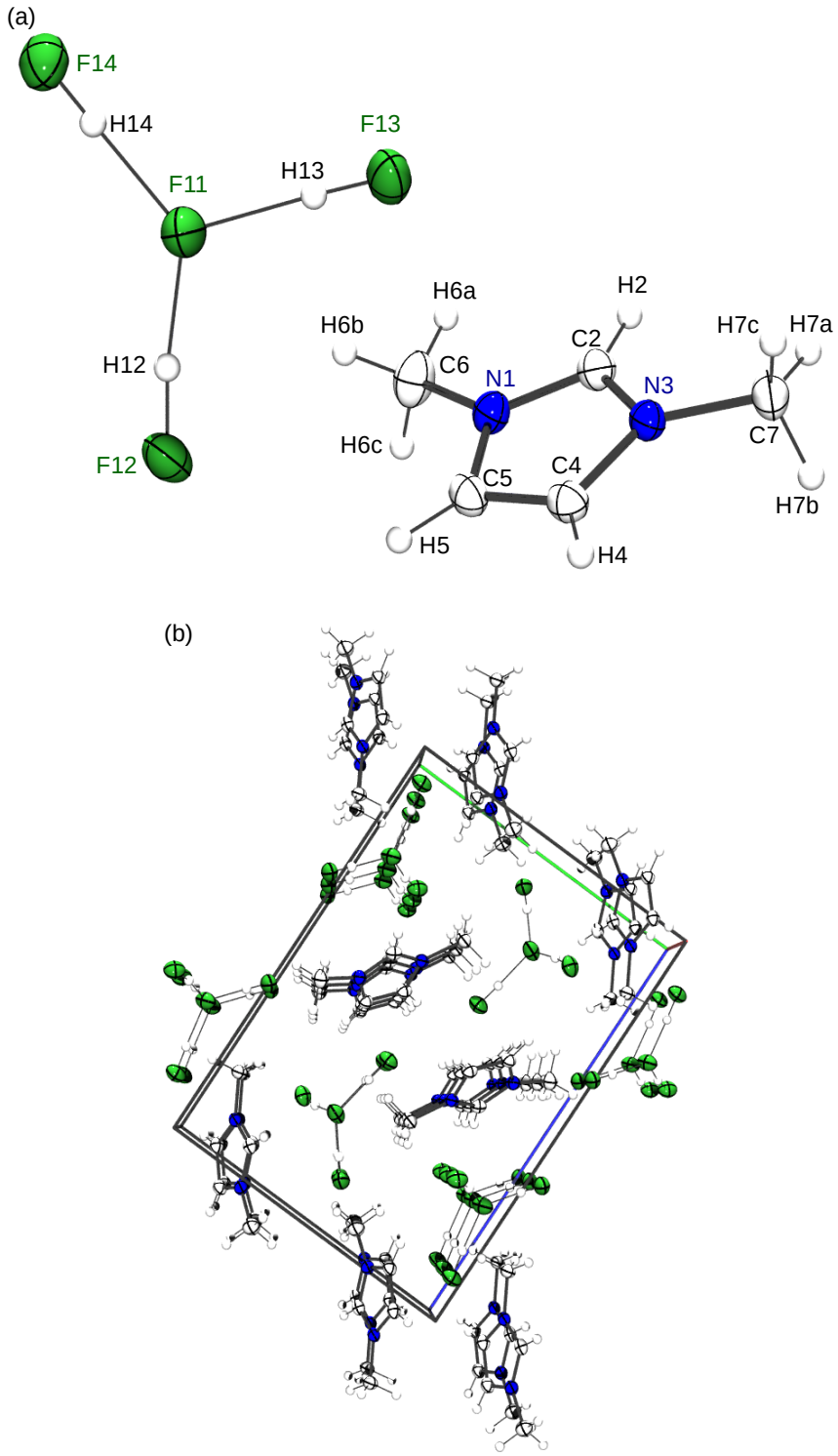

Figure 5. Crystal structure of DMIm(FH)$_3$F; (a) asymmetric unit and (b) Crystal packing.

The $(FH)_2F^-$ ion in DMIm(FH)$_2$F adopts a bent geometry (roughly C_{2v} symmetry). The F11−F12 and F11−F13 bond lengths of 2.333(4) and 2.305(4) Å and the F12−F11−F13 bond angle of 134.96(17)° agree with those of $(FH)_2F^-$ previously determined in some compounds including K(FH)$_2$F[45] and $(CH_3)_4N(FH)_2F$[46]. The $(FH)_3F^-$ ion in DMIm(FH)$_3$F adopts a slightly distorted trigonal planar geometry

as is found in $K(FH)_3F$[47], although the chain-like $(FH)(FHF)(HF)^-$ is also known as a structural isomer in $K(FH)_{2.5}F$[47]. The F11−F12, F11−F13, and F11−F14 bond lengths of 2.3822(10), 2.3871(10), and 2.4058(10) Å agree with those of $(FH)_3F^-$ previously determined in some compounds including $K(FH)_3F$[47] and $(CH_3)_4N(FH)_3F$[46], and are longer than the F−F bond lengths in $(FH)_2F^-$ because of the lower covalency in the F−H bond of $(FH)_3F^-$. Most geometrical parameters of $(FH)_2F^-$ and $(FH)_3F^-$ are reproduced well by quantum mechanical calculation at MP2/aug-cc-pVTZ (see Table 2). The three bond angles, F12−F11−F13 (108.75(4)º), F13−F11−F14 (115.72(4)º), and F14−F11−F12 (133.18(4)º), determined in the crystal structure are not equivalent to each other and deviates from the ideal angle (120º), which is probably due to the effects of crystal packing. The cations and anions in $DMIm(FH)_2F$ and $DMIm(FH)_3F$ form one-dimensional columns as is observed in crystal structures of some imidazolium-based salts (*e.g.* BMImCl[36], EMImFHF[33], and $DMImOSO_2OCH_3$[44]). Table 3 is the list of hydrogen bonds between the H2, H4, or H5 and the anion. The distances (2.2 - 2.5 Å) are much shorter than the sum of the van der Waals radii of the hydrogen and fluorine atoms (2.7 Å). Characteristics of these short contacts will be discussed below.

Table 3. Hydrogen bonding geometries for $DMIm(FH)_2F$ and $DMIm(FH)_3F$ (Å, deg.)

D−H···*A*	*D*−H	H···*A*	*D*···*A*	*D*−H···*A*
$DMIm(FH)_2F$				
C2−H2···F12	0.93	2.535	2.961(5)	108.27
C2−H2···F13	0.93	2.361	3.124(5)	139.13
C5−H5···F13	0.93	2.476	3.295(6)	146.92
$DMIm(FH)_3F$				
C2−H2···F12	0.93	2.209	3.1067(13)	161.81
C4−H4···F13	0.93	2.445	3.0710(12)	124.67
C4−H4···F13	0.93	2.426	3.2456(13)	146.94

Interaction energies of ion pairs.

(a) Interaction energies in the crystal structures. Figure 6 shows interaction energies calculated at the MP2/6-311G** level for ion pairs in EMImFHF[33], $DMIm(FH)_2F$, and $DMIm(FH)_3F$ against the reciprocal distances between the cation and anion. Assuming the cation and anion as the positive and negative point charges, the Coulomb interaction energies calculated by Coulomb's law (eq. (1)) are also shown in this figure with a dashed line.

$$E = z_+ z_- e^2 / 4\pi\varepsilon R \qquad (1)$$

Here, z_+ and z_- are the valences of the cation and anion, respectively, e is the elementary charge, ε is permittivity, and R is the distance between the cation and anion. The midpoint between the two nitrogen atoms of each imidazolium ring was used as the center of the cation.[32] The centers of the anions are positioned at the hydrogen atom for FHF^-, at the midpoint of the two hydrogen atoms for $(FH)_2F^-$, and at the central fluorine atom for $(FH)_3F^-$, respectively.

The calculated interaction energies are nearly inversely proportional to the distance, which suggests the ion-ion interaction energies in these crystal structures are dominated by electrostatic interaction. There is a gap between the ion-ion interaction energies and the ideal Coulomb interaction energies in the plotted R^{-1} range. This gap may result from the attraction of the dipoles and the induced dipoles due to the strong electric field produced by the ions, including hydrogen bonding. These observations suggest that hydrogen bonding between the cation and anion do not largely contribute to the interactions between the ions.

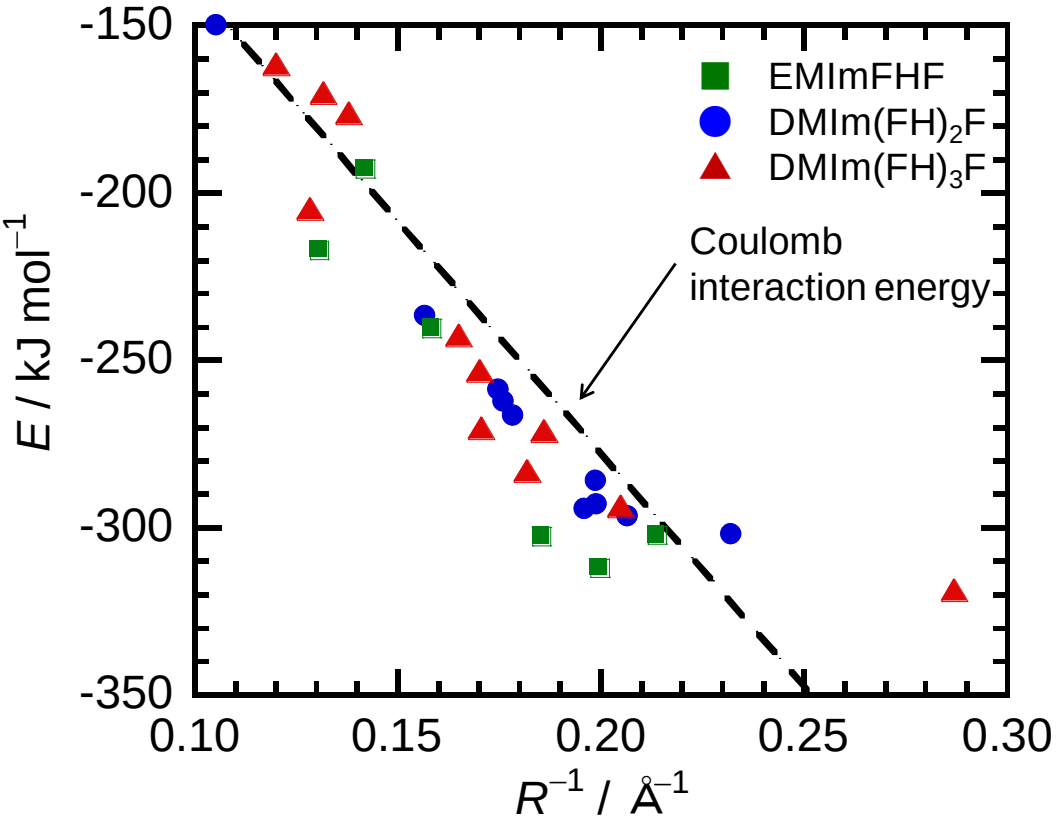

Figure 6. Interaction energies (E) for the $EMIm^+$-FHF^-, $DMIm^+$-$(FH)_2F^-$, and $DMIm^+$-$(FH)_3F^-$ ion pairs in the crystal structures against the reciprocal distances between the cation and anion (R^{-1}). The energies were calculated at the MP2/6-311G** level. The dashed line is Coulomb interaction energy calculated by the Coulomb's law (eq. (1)), assuming the cation and anion as the positive and negative point charges.

(b) Orientation dependence of the interaction energies. In order to evaluate the characteristics of hydrogen bonds in the dialkylimidazolium cation and fluorohydrogenate anion, directionality of the hydrogen bonds were evaluated by calculating the interaction energies of several typical configurations at the MP2/6-311G** level for the $DMIm^+$-FHF^- ion pair (see Figures S1 and S2 in Supporting Information for the results at the MP2/aug-cc-pVTZ level and Figures S5 and S6 for the calculations for the HF oligomers in which the typical hydrogen bonding exists). Figure 7 shows the six orientations of the $DMIm^+$-FHF^- ion pairs calculated to examine the interaction energies. Figure 8 shows the calculated energies against the distance between the cation and anion. Although the C2−H bond does not point toward the fluorine atom, the orientation (c) (399 kJ mol^{-1}) is more stable than the orientation (a) (362 kJ mol^{-1}) because of the short cation-anion contact in the orientation (c). The interaction energy of the

orientation (c) is larger than that of the orientation (b) (375 kJ mol^{-1}), which may arise from the attraction between the hydrogen atom of the methyl group and the fluorine atom. Although the FHF^- ion in the orientations (d) and (f) are not involved with hydrogen bonding, their interaction energies (359 and 370 kJ mol^{-1}) are similar to that of the orientation (a) (362 kJ mol^{-1}). These results also support that the interaction energy is mainly determined by Coulomb interaction and hydrogen bonding is not a decisive factor to reach energy minimum. The gap between the potential curve (a) and the ideal Coulomb interaction in the large *R* region (> 3.5 Å) results from the interactions of the dipoles and the induced dipoles. The gap between the curves (d), (e), or (f) and the ideal Coulomb interaction is caused by the repulsion between the negative charge on the anion and π electron cloud on the imidazolium ring. These results agree with the case for the DMIm-BF_4 ion pair.[32]

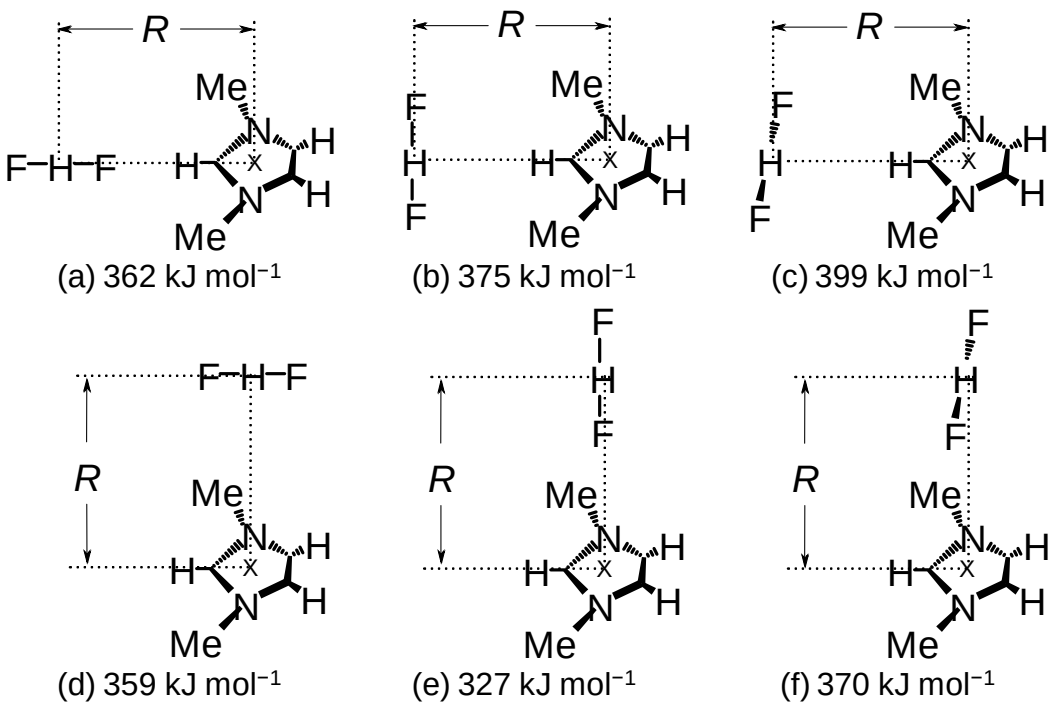

Figure 7. Six orientations of the $DMIm^+$-FHF^- ion pairs calculated to examine the interaction energies. The number below the structure is the interaction energy at the minimum in the potential curve at the MP2/6-311G** level. X is the midpoint between the two nitrogen atoms close to the center of the positive charge of the imidazolium ring.

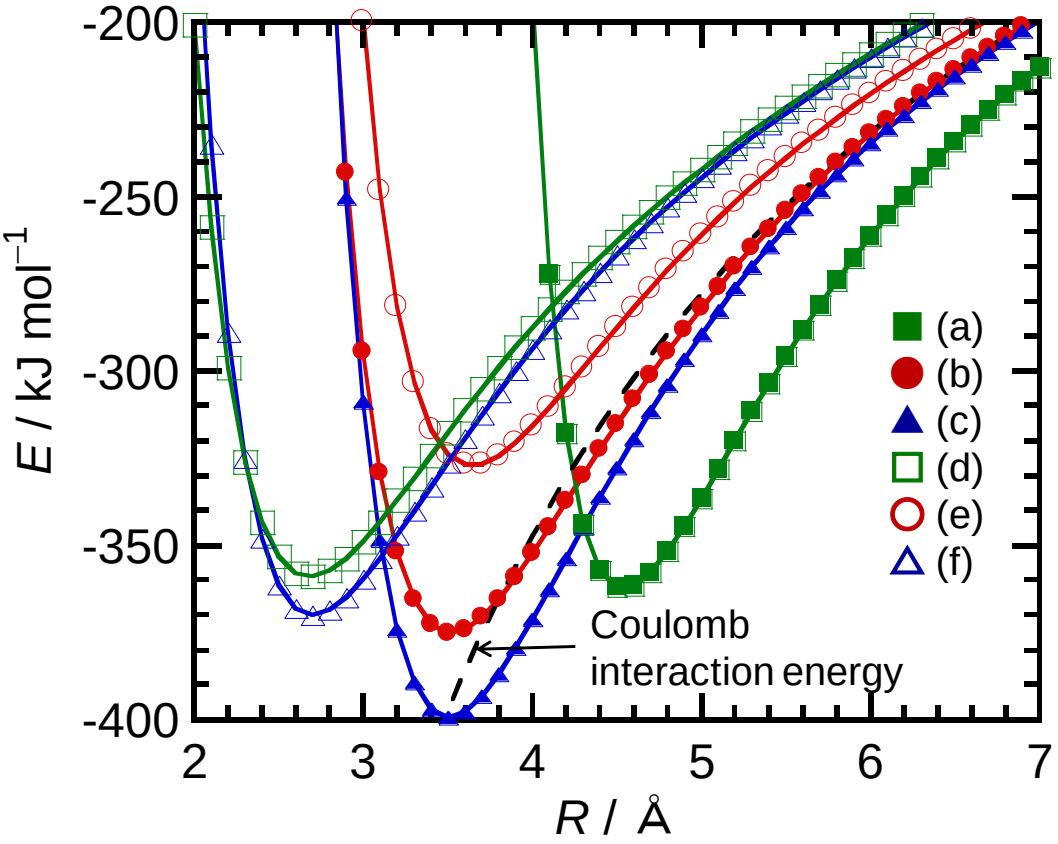

Figure 8. Interaction energies (*E*) for the six $DMIm^+$-FHF^- ion pairs shown in Figure 7 (MP2/6-311G** level) against the distances between the cation and the anion (*R*). The geometries of the cation and anion independently optimized at the same level were used. The dashed line is Coulomb interaction energy calculated by the Coulomb's law (eq. (1)), assuming the cation and anion as the positive and negative point charges.

Ion conduction mechanism of fluorohydrogenate ILs. The results of the aforementioned calculation for the interaction energy between the imidazolium cation and fluorohydrogenate anion indicate that the static cation-anion interactions in the fluorohydrogenate salts are not special compared to those in other imidazolium salts and is mainly dominated by electrostatic interaction.[32] In other words, the low viscosity and high conductivity of fluorohydrogenate ILs are not derived from the static but from the dynamic aspect in the liquid state.

Molar conductivity of ILs is related to diffusion coefficient via the Nernst-Einstein equation (eq. (2)) if the component ions are totally dissociated.[21-25]

$$\Lambda = N_A e^2(\nu_+ z_+^2 D_+ + \nu_- z_-^2 D_-) / kT \qquad (2)$$

Here, N_A is the Avogadro number, ν_+ and ν_- are the numbers of the cations and anions per formula unit, respectively, D_+ and D_- are the diffusion coefficients of the cation and anion, respectively, k is the Boltzmann constant, and T is absolute temperature. According to the general rule based on the Stokes-Einstein equation (eq. (3)), diffusion coefficients of ionic species in ILs increase with decrease in size of the ions.

$$D = kT / 6\pi\eta r \qquad (3)$$

Here, η is viscosity and r is Stokes radius. On the other hand, when the size of ions becomes too small (*e.g.* halide salts), the Coulomb interaction between the cation and anion becomes large, resulting in the increase in viscosity and decrease in diffusion coefficient.

Comparison of molar conductivity between $EMImN(CN)_2$ (4.4 S cm^2 mol^{-1} at 20^{o}C) and $EMImC(CN)_3$ (3.3 S cm^2 mol^{-1} at 20^{o}C) gives a simple example to see the effect of the size based on eq. (3).[48] On the contrary, molar conductivity of $EMIm(FH)_nF$ ($1.3 < n < 2.3$) exhibits an opposite trend and monotonously increases as the HF composition in the anion (n), that is, the size of the anion, increases (*e.g.* 6.4 S cm^2 mol^{-1} for n = 1.3, 9.6 S cm^2 mol^{-1} for n = 1.8, and 15.6 S cm^2 mol^{-1} for n = 2.3[11] at 25^{o}C (see Table S12 in Supporting Information for densities and ionic conductivities used for estimating these molar conductivities)), although there is a structural resemblance between some of the $(FH)_nF^-$ anions and $N(CN)_2^-$ or $C(CN)_3^-$. The activation energy values of ionic conductivity for $EMIm(FH)_nF$ (*e.g.* 13.9 kJ mol^{-1} for n = 1.3, 12.7 kJ mol^{-1} for n = 1.8, and 10.0 kJ mol^{-1} for n = 2.3[11]) also reflect this trend (see Table S10 in Supporting Information for ionic conductivities used for calculating these activation energies).

The ^{1}H-NMR and ^{19}F-NMR spectra of fluorohydrogenate ILs show only one signal assigned to the fluorohydrogenate anions even at −40^{o}C.[10] This observation suggests that the HF units in $(FH)_nF^-$

exchange between the fluorohydrogenate anions with the speed faster than the NMR time-scale, suggesting the anionic structures such as $(FH)_2F^-$ and $(FH)_3F^-$ are rather flexible in the liquid state whereas they are rigid in the solid states as found in the crystal structures (see Figures 4 and 5).

Diffusion coefficients of the ionic species in fluorohydrogenate ILs were obtained by PGSE-NMR (*e.g.* $D_+ = 3.0\times10^{-6}$ cm^2 s^{-1} and $D_- = 4.1\times10^{-6}$ cm^2 s^{-1} in EMIm$(FH)_{2.3}$F).[49] These diffusion coefficients are much larger than those in other ILs (*e.g.* $D_+ = 0.50\times10^{-6}$ cm^2 s^{-1} and $D_- = 0.42\times10^{-6}$ cm^2 s^{-1} in $EMImBF_4$).[21] Although the diffusion coefficient of the anion is larger than that of the cation in fluorohydrogenate ILs, the diffusion coefficient of the cation in fluorohydrogenate ILs is remarkably larger than those in other ILs, namely, both the cation and anion in fluorohydrogenate ILs migrate faster than those in other ILs.

Fluorohydrogenate anion formed by the reaction of strong Brønsted base fluoride ion and weak acid hydrogen fluoride is a weak Brønsted acid in which proton is coordinated by two fluoride anions and not easily released. Therefore special conduction mechanism such as proton hopping based on the Grotthus mechanism is ruled out in fluorohydrogenate ILs. Although fluoride ion hopping is another possibility, the viscosities of fluorohydrogenate ILs are low enough to satisfy the Walden rule (*cf.* compare EMIm$(FH)_{2.3}$F (η = 4.9 cP, Λ = 15.6 S cm^2 mol^{-1})[11] with $EMImBF_4$ (η = 34 cP, Λ = 2.0 S cm^2 mol^{-1})[17]).

Based on these facts, the high conductivity of fluorohydrogenate ILs is considered to be derived from the cation-anion interaction weakened by the HF units exchanging between the $(FH)_nF^-$ anions. Figure 9 shows a proposed ion conduction model in fluorohydrogenate ILs. The anionic species actually diffusing in fluorohydrogenate ILs is smaller than the species observed by IR spectroscopy, FHF^- for example. These smaller anions are produced in a very short period, resulting from the exchange of the HF unit. On the other hand, the HF unit which appears during the exchanging process between the anions behaves like a solvent molecule with a certain dielectric moment to weaken the Coulomb interactions between the ions (see eq. (1)). Nevertheless, there is no HF dissociation pressure on fluorohydrogenate ILs at the n value less than a certain HF composition (*e.g.* $n < 2.3$ for alkylimidazolium systems), which suggests a completely free HF molecule does not exist or its lifetime

is extremely short. This model can explain the large diffusion coefficients of cations in fluorohydrogenate ILs, since the weaker Coulomb interaction make the cation freer as well. Transport number of the anion is usually smaller than that of the cation in ILs,[21] whereas the opposite trend was reported for fluorohydrogenate ILs.[49] This unusual property of fluorohydrogenate ILs probably results from the small anionic diffusion species in fluorohydrogenate ILs. Increase in ionic conductivity with increase in *n* is also explained by this model. The HF dissociation energies calculated at the MP2/aug-cc-pVTZ level are 157.2 kJ mol^{-1} for FHF^-, 85.0 kJ mol^{-1} for $(FH)_2F^-$, and 51.2 kJ mol^{-1} for $(FH)_3F^-$ (see Table S8 in Supporting Information for the results at the other levels). This result suggests that the HF dissociation becomes easier and a large number of HF units exist in ILs as *n* becomes large, contributing to the decrease in Coulomb interaction.

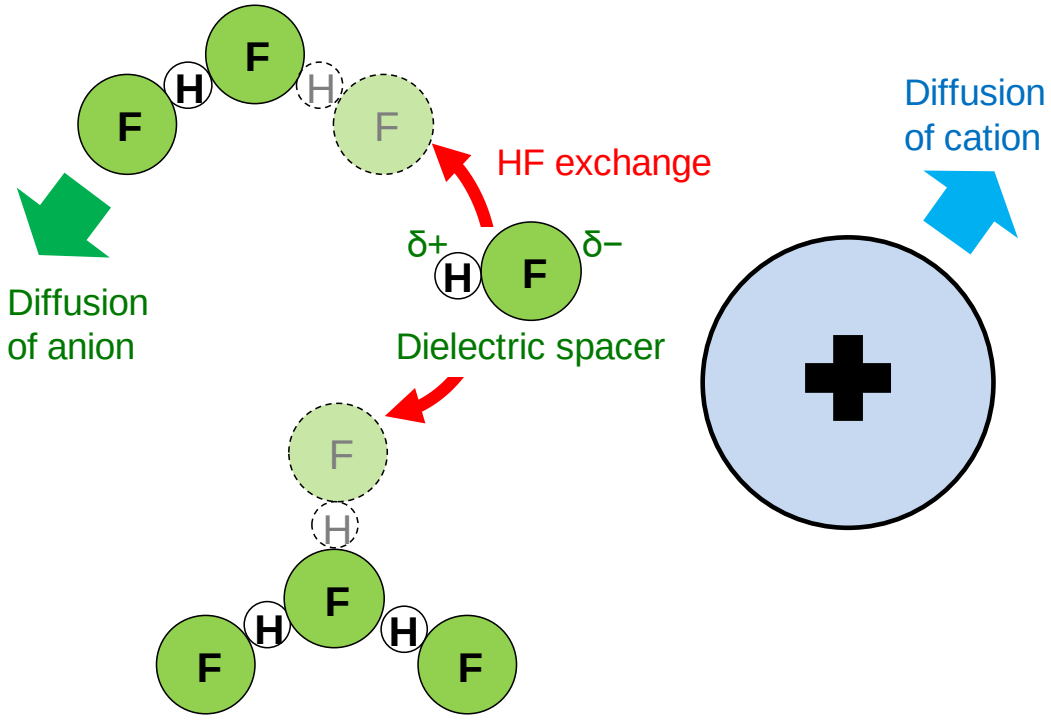

Figure 9. Model for the ion conduction mechanism of fluorohydrogenate ILs.

Conclusions

The origin of low viscosity and high conductivity for fluorohydrogenate ILs was studied from structural and physicochemical aspects. The 1,3-dimethylimidazolium salts, $DMIm(FH)_{2.3}F$, DMImFHF, $DMIm(FH)_2F$, and $DMIm(FH)_3F$ were prepared and characterized by DSC, X-ray diffraction

measurements, and quantum mechanical calculations. The interaction energies for the ion pairs in the crystal structures of EMImFHF, $DMIm(FH)_2F$, and $DMIm(FH)_3F$ and for the $DMIm^+$-FHF^- ion pairs in several orientations were evaluated by quantum mechanical calculations. These calculations show that the cation-anion interaction is mainly determined simply by the distance between the cation and anion and dominated by electrostatic interactions. Hydrogen bonding between the cation and anion is not a decisive factor to reach energy minimum as reported for other imidazolium salts. From the results of the NMR spectra, ionic conductivity, and self diffusion coefficients of $EMIm(FH)_nF$, the low viscosity and high conductivity of fluorohydrogenate ILs are derived from the weak interaction between the cation and anion because the HF units exchanging between the $(FH)_nF^-$ anions work as dielectric spacers.

Experimental

Apparatus and Materials. Moisture sensitive materials were handled in a glove box. A vacuum line was constructed of stainless steel to handle corrosive gases. The line was connected to a rotary vacuum pump through a soda lime chemical trap connected to a glass cold trap in series. The tetrafluoroethylene-perfluoroalkylvinylether copolymer (PFA) reactor connected to a stainless steel valve with a Kel-F tip was used as a reaction vessel. Anhydrous hydrogen fluoride, aHF (Stella Chemifa Corp., purity 99.9%), was dried over K_2NiF_6 (Ozark-Mahoning Co.) for several days prior to use. Chloromethane (Wako Pure Chemical Industries, Ltd., purity > 98%), 1-methylimidazole (Sigma-Aldrich Co., purity ≥ 99%, water content ≤ 50 ppm), acetonitrile (Wako Pure Chemical Industries, Ltd., purity ≥ 99%, water content ≤ 50 ppm), ethyl acetate (Wako Pure Chemical Industries, Ltd., purity ≥ 99.5%, water content ≤ 50 ppm), and 1-ethyl-3-methylimidazolium fluorohydrogenate ILs, $EMIm(FH)_{1.3}F$ and $EMIm(FH)_{2.3}F$, for density measurements (Morita Chemical Industries Co., Ltd.) were used as purchased. $EMIm(FH)_{1.8}F$ for density measurement was prepared by the stoichiometric reaction of $EMIm(FH)_{1.3}F$ with $EMIm(FH)_{2.3}F$. The chloride, 1,3-dimethylimidazolium chloride (DMImCl), was prepared by the reaction of 1-methylimidazole and chloromethane as described in the previous work.[13]

Synthesis. Fluorohydrogenate ILs were prepared according to the literature method.[11,12] The obtained DMImCl was weighed and loaded in a PFA tube under a dry argon atmosphere, followed by reaction with a large excess of aHF at room temperature. Elimination of the volatile gases at 25°C gave $DMIm(FH)_{2.3}F$.[11] The bifluoride salt, DMImFHF, was crystallized from an HF-deficient salt obtained by evacuating HF from $DMIm(FH)_{2.3}F$ at around 120°C.[33] The obtained crystals were separated from the liquid by soaking up the liquid using Kimwipe thoroughly dried at 150°C under vacuum for one day. The salt, $DMIm(FH)_2F$, was prepared by mixing $DMIm(FH)_{2.3}F$ with the HF-deficient salt which was prepared by placing $DMIm(FH)_{2.3}F$ at elevated temperatures under dynamic vacuum.[12] The HF composition '*n*' was confirmed by elemental analysis and IR spectra. $EMIm(FH)_{2.3}F$ for ionic conductivity measurement was synthesized by the metathesis of EMImCl and large excess of aHF. $EMIm(FH)_{1.3}F$ and $EMIm(FH)_{1.8}F$ were prepared by pyrolysis of $EMIm(FH)_{2.3}F$ under dynamic vacuum at 125 and 80°C, respectively.[12]

Analysis. Thermal analyses for determination of phase transition temperatures were performed by a differential scanning calorimeter, DSC-60 (Shimadzu Corp.) under a dry argon gas flow (50 mL min^{-1}). Samples were sealed in stainless steel cells using a high-pressure sealing machine in a glove box. The atmosphere around the cell was purged with dry argon gas during the measurement. A scan rate of 5°C min^{-1} was selected. Thermal decomposition temperature of DMImFHF was measured by a thermogravimetric analyzer, DTG-60H (Shimadzu Corp.) under a dry argon gas flow (50 mL min^{-1}). Platinum cells used for the measurement were washed with acetone just before the measurement and dried in the apparatus at 200°C for 10 minutes. The temperature was scanned from 150 to 350°C with a heating rate of 1°C min^{-1} after drying at 150°C for 3 hours. Ionic conductivity measurements of DMImFHF, $EMIm(FH)_{1.3}F$, and $EMIm(FH)_{1.8}F$ were performed with the aid of PARSTAT 2273 (Princeton Applied Research) or HZ-3000 (Hokuto Denko) electrochemical measurement systems. Ionic conductivity was measured by an AC impedance technique using a cell with platinum disk electrodes calibrated using KCl standard aqueous solutions. Densities of $EMIm(FH)_{1.3}F$ and $EMIm(FH)_{1.8}F$ were measured by weighing the sample in a calibrated PFA vessel. Infra-red spectra of DMImCl, DMImFHF,

and $DMIm(FH)_2F$ were obtained by an FT-IR spectrometer, FTS-155 (BIO-RAD). The sample was sandwiched between a pair of AgCl windows fixed in a stainless airtight cell.

X-Ray Diffraction Analysis.

(a) Powder Diffraction. Capillaries used for X-ray diffraction measurements were dried under vacuum at 500°C. The crystalline sample of DMImFHF was transferred into a quartz capillary (Overseas X-Ray Service Co., Ltd.) in a glove box. The capillary was temporarily plugged with silicone grease, and then flame-sealed outside the glove box using an oxygen microburner. The sample was centered on an X-ray diffractometer, R-AXIS RAPID-II (Rigaku Corp.), equipped with an imaging plate area detector and graphite-monochromated MoKα radiation (λ = 0.71073 Å). The RAPID XRD 2.3.3[50] was used to control the diffractometer and the ϕ angle was rotated at a rate of 1^{o} s^{-1} during data collection (720 seconds). The temperature of the sample was controlled by dry nitrogen flow.

(b) Single-Crystal Diffraction. Single crystals of $DMIm(FH)_2F$ were grown by cooling the liquid sample from 25°C to −15°C. In the case of $DMIm(FH)_3F$, a stoichiometric amount of HF was added on $DMIm(FH)_{2.3}F$ using a mass flow meter, 8300MM-0-1 (KOFLOC), and the obtained liquid $DMIm(FH)_3F$ was cooled from 25°C to −60°C to grow crystals. In both the cases, a selected crystal was picked up with a glass pin under a dry nitrogen flow (below −70°C) and mounted to a goniometer head on the diffractometer, R-AXIS RAPID-II, using the cryotongs. The data collection was performed using graphite-monochromated MoKα radiation (λ = 0.71073 Å) under a cold stream of nitrogen gas (−173°C). The output was 40 mA at 50 kV. The RAPID AUTO 2.40[51] was used to process data. The SIR-92[52] and SHELXL-97[53] were used for solution and refinement of the structure, respectively, through the WinGX interface[54]. Anisotropic displacement factors were introduced for all atoms except for hydrogen. The position of the hydrogen atoms in the anions were optimized with isotropic displacement factors. The hydrogen atoms in the cations were refined using an appropriate riding model. For $DMIm(FH)_2F$, the ROTAX[55] was used for twinning detection because of a high *R* value and an inappropriate structure obtained. The twinning matrix of [−1 0 0 −1 0 1 −1 1 0] and an estimated domain ratio of 0.47:0.53 were obtained and used for the final refinement.

Quantum Mechanical Calculation. The Gaussian 03 program[56] was used for quantum mechanical calculations. The optimized geometries, volumes, and vibrational data of fluorohydrogenate anions, hydrogen fluoride, and $DMIm^+$ were calculated at B3LYP, PBE1PBE, MPW1PW91, and MP2 levels of theory using 6-311G**, cc-pVTZ, and aug-cc-pVTZ basis sets. The volume of F^- was also calculated at the same levels. The NBO analyses were performed for the B3LYP, PBE1PBE, and MPW1PW91 optimized local minima.[57-60] Interaction energies between the imidazolium cation and neighboring fluorohydrogenate anions were calculated at MP2/6-311G** level for the ion pairs determined in the crystal structures (EMImFHF[33], $DMIm(FH)_2F$, and $DMIm(FH)_3F$). Interaction energies were calculated at MP2/6-311G** and MP2/aug-cc-pVTZ levels for the ion pairs of $DMIm^+$ and FHF^- with fixed distances for several orientations, where the structure optimized in the gas phase was used for each ion. The basis set superposition error (BSSE)[61] for the ion pair was corrected using the counterpoise method.[62] The interaction between HF molecules were also calculated at MP2/6-311G** and MP2/aug-cc-pVTZ levels for HF oligomers to examine the typical hydrogen bond.

Acknowledgements

This work was financially supported by Grant-in-Aid for Scientific Research for Priority Area "Science of Ionic Liquids" of MEXT and Grant-in-Aid for Scientific Research of JSPS, #20246140. The authors would like to thank Dr. Seiji Tsuzuki of National Institute of Advanced Industrial Science and Technology for his kind help in quantum mechanical calculations.

Supporting Information Available: Calculated geometrical parameters, partial atomic charges, volumes, HF dissociation energies, hydrogen bonding and ion-ion interaction energies, experimental and calculated vibrational frequencies and intensities, X-ray powder diffraction data, conductivities, Arrhenius equation parameters, densities and molar conductivities, TG trace, IR spectra, and additional relevant literature. This material is available free of charge via the Internet at http://pubs.acs.org.

References

(1) Wilkes, J. S. *Green Chem.* **2002**, *4*, 73.

(2) Seddon, K. R. *J. Chem. Technol. Biotechnol.* **1997**, *68*, 351.

(3) Wasserscheid, P.; Keim, W. *Angew. Chem. Int. Ed.* **2000**, *39*, 3772.

(4) Hagiwara, R.; Ito, Y. *J. Fluorine Chem.* **2000**, *105*, 221.

(5) Welton, T. *Chem. Rev.* **1999**, *99*, 2071.

(6) Xue, H.; Verma, R.; Shreeve, J. M. *J. Fluorine Chem.* **2006**, *127*, 159.

(7) Hagiwara, R.; Lee, J. S. *Electrochemistry* **2007**, *75*, 23.

(8) Ohno, H. *Electrochemical Aspects of Ionic Liquids*; John Wiley and Sons, Inc.: Hoboken, NJ, 2005.

(9) Hagiwara, R.; Hirashige, T.; Tsuda, T.; Ito, Y. *J. Fluorine Chem.* **1999**, *99*, 1.

(10) Hagiwara, R.; Hirashige, T.; Tsuda, T.; Ito, Y. *J. Electrochem. Soc.* **2002**, *149*, D1.

(11) Hagiwara, R.; Matsumoto, K.; Nakamori, Y.; Tsuda, T.; Ito, Y.; Matsumoto, H.; Momota, K. *J. Electrochem. Soc.* **2003**, *150*, D195.

(12) Hagiwara, R.; Nakamori, Y.; Matsumoto, K.; Ito, Y. *J. Phys. Chem. B* **2005**, *109*, 5445.

(13) Matsumoto, K.; Hagiwara, R.; Ito, Y. *Electrochem. Solid State Lett.* **2004**, *7*, E41.

(14) Matsumoto, K.; Hagiwara, R. *Electrochemistry* **2005**, *73*, 730.

(15) Yamagata, M.; Konno, S.; Matsumoto, K.; Hagiwara, R. *Electrochem. Solid State Lett.* **2009**, *12*, F9.

(16) Kanematsu, S.; Matsumoto, K.; Hagiwara, R. *Electrochem. Comm.* **2009**, *11*, 1312.

(17) Ohtsuki, J.; Matsumoto, K.; Hagiwara, R. *Electrochemistry* **2009**, *77*, 624.

(18) Ue, M.; Takeda, M.; Toriumi, A.; Kominato, A.; Hagiwara, R.; Ito, Y. *J. Electrochem. Soc.* **2003**, *150*, A499.

(19) Hagiwara, R.; Nohira, T.; Matsumoto, K.; Tamba, Y. *Electrochem. Solid State Lett.* **2005**, *8*, A231.

(20) Senda, A.; Matsumoto, K.; Nohira, T.; Hagiwara, R. *J. Power Sources*, *195*, 4414.

(21) Noda, A.; Hayamizu, K.; Watanabe, M. *J. Phys. Chem. B* **2001**, *105*, 4603.

(22) Tokuda, H.; Hayamizu, K.; Ishii, K.; Abu Bin Hasan Susan, M.; Watanabe, M. *J. Phys. Chem. B* **2004**, *108*, 16593.

(23) Tokuda, H.; Hayamizu, K.; Ishii, K.; Susan, M.; Watanabe, M. *J. Phys. Chem. B* **2005**, *109*, 6103.

(24) Tokuda, H.; Ishii, K.; Susan, M.; Tsuzuki, S.; Hayamizu, K.; Watanabe, M. *J. Phys. Chem. B* **2006**, *110*, 2833.

(25) Tokuda, H.; Tsuzuki, S.; Susan, M.; Hayamizu, K.; Watanabe, M. *J. Phys. Chem. B* **2006**, *110*, 19593.

(26) Angell, C. A.; Byrne, N.; Belieres, J. P. *Acc. Chem. Res.* **2007**, *40*, 1228.

(27) Xu, W.; Cooper, E. I.; Angell, C. A. *J. Phys. Chem. B* **2003**, *107*, 6170.

(28) Yoshizawa, M.; Xu, W.; Angell, C. A. *J. Am. Chem. Soc.* **2003**, *125*, 15411.

(29) Turner, E. A.; Pye, C. C.; Singer, R. D. *J. Phys. Chem. A* **2003**, *107*, 2277.

(30) Hunt, P. A.; Gould, I. R. *J. Phys. Chem. A* **2006**, *110*, 2269.

(31) Tsuzuki, S.; Tokuda, H.; Hayamizu, K.; Watanabe, M. *J. Phys. Chem. B* **2005**, *109*, 16474.

(32) Tsuzuki, S.; Tokuda, H.; Mikami, M. *Phys. Chem. Chem. Phys.* **2007**, *9*, 4780.

(33) Matsumoto, K.; Tsuda, T.; Hagiwara, R.; Ito, Y.; Tamada, O. *Solid State Sci.* **2002**, *4*, 23.

(34) Matsumoto, K.; Hagiwara, R. *J. Fluorine Chem.* **2007**, *128*, 317.

(35) Dymek, C. J.; Grossie, D. A.; Fratini, A. V.; Adams, W. W. *J. Mol. Struct.* **1989**, *213*, 25.

(36) Saha, S.; Hayashi, S.; Kobayashi, A.; Hamaguchi, H. *Chem. Lett.* **2003**, *32*, 740.

(37) Salanne, M.; Simon, C.; Turq, P. *J. Phys. Chem. B* **2006**, *110*, 3504.

(38) Bhargava, B. L.; Balasubramanian, S. *J. Phys. Chem. B* **2008**, *112*, 7566.

(39) Salanne, M.; Simon, C.; Turq, P. *J. New Mater. Electrochem. Syst.* **2006**, *9*, 291.

(40) Winsor, R. V.; Cady, G. H. *J. Am. Chem. Soc.* **1948**, *70*, 1500.

(41) Cady, G. H. *J. Am. Chem. Soc.* **1934**, *56*, 1431.

(42) Holbrey, J. D.; Reichert, W. M.; Nieuwenhuyzen, M.; Sheppard, O.; Hardacre, C.; Rogers, R. D. *Chem. Commun.* **2003**, 476.

(43) Holbrey, J. D.; Reichert, W. M.; Rogers, R. D. *Dalton Trans.* **2004**, 2267.

(44) Holbrey, J. D.; Reichert, W. M.; Swatloski, R. P.; Broker, G. A.; Pitner, W. R.; Seddon, K. R.; Rogers, R. D. *Green Chem.* **2002**, *4*, 407.

(45) Forrester, J. D.; Templeton, D. H.; Zalkin, A.; Senko, M. E. *Acta Cryst.* **1963**, *16*, 58.

(46) Mootz, D.; Boenigk, D. *Z. Anorg. Allg. Chem.* **1987**, *544*, 159.

(47) Mootz, D.; Boenigk, D. *J. Am. Chem. Soc.* **1986**, *108*, 6634.

(48) Yoshida, Y.; Muroi, K.; Otsuka, A.; Saito, G.; Takahashi, M.; Yoko, T. *Inorg. Chem.* **2004**, *43*, 1458.

(49) Saito, Y.; Hirai, K.; Matsumoto, K.; Hagiwara, R.; Minamizaki, Y. *J. Phys. Chem. B* **2005**, *109*, 2942.

(50) *RAPID XRD*, version 2.3.3; Rigaku Corporation: Tokyo, Japan, 1999.

(51) *RAPID AUTO*, version 2.40; Rigaku Corporation: Tokyo, Japan, 2006.

(52) Altomare, A.; Cascarano, G.; Giacovazzo, C.; Guagliardi, A. *J. Appl. Crystallogr.* **1993**, *26*, 343.

(53) Sheldrick, G. M. *Acta Cryst. A* **2008**, *64*, 112.

(54) Farrugia, L. J. *J. Appl. Crystallogr.* **1999**, *32*, 837.

(55) Cooper, R. I.; Gould, R. O.; Parsons, S.; Watkin, D. J. *J. Appl. Crystallogr.* **2002**, *35*, 168.

(56) Frisch, M. J.et al. *Gaussian 03*, Revision E.01; Gaussian, Inc.: Pittsburgh, PA, 2003.

(57) Reed, A. E.; Weinstock, R. B.; Weinhold, F. *J. Chem. Phys.* **1985**, *83*, 735.

(58) Reed, A. E.; Curtiss, L. A.; Weinhold, F. *Chem. Rev.* **1988**, *88*, 899.

(59) Glendening, E. D.; Reed, A. E.; Carpenter, J. E.; Weinhold, F. *NBO*, version 3.1; Gaussian, Inc.: Pittsburgh, PA, 1990.

(60) Glendening, E. D.; Badenhoop, J. K.; Reed, A. E.; Carpenter, J. E.; Bohmann, C. M.; Morales, C. M.; Weinhold, F. *NBO*, version 5.0; Theoretical Chemistry Institute, University of Wisconsin: Madison, WI, 2001.

(61) Ransil, B. J. *J. Chem. Phys.* **1961**, *34*, 2109.

(62) Boys, S. F.; Bernardi, F. *Mol. Phys.* **1970**, *19*, 553.

Table of Contents (TOC) Image

Ion-ion interactions of and conduction mechanism of highly conductive fluorohydrogenate ionic liquids